Decoding the interplay between tidal notch geometry and sea-level variability during the Last Interglacial (Marine Isotopic Stage 5e) high stand

N. Georgiou[1,2*], P. Stocchi[3], E. Casella[1], A. Rovere[1]

[1] Ca’ Foscari University of Venice, Department of Environmental Sciences, Informatics and Statistics, Scientific Campus, via Torino 155, 30172 Mestre (VE), Italy.

[2] University of Patras, Department of Geology, Panepistimioupoli, 265 04 Rio, Patra, Greece.

[3] Dipartimento di Scienze Pure e Applicate (DiSPeA), Università degli Studi di urbino "Carlo Bo", Via Aurelio Saffi 2, 61029, Urbino PU, Italy.

*Corresponding author: Nikos Georgiou (nikos.georgiou@unive.it)

Key Points:

- Tidal notch geometry provides continuous insight into past sea-level variability utilizing a cliff erosion model & Monte Carlo analysis
- Notch’s geometry can be replicated both through simultaneous or asynchronous Antarctic-Greenland ice-melting scenarios
- Higher-than-present erosion rates and a 6m sea-level peak replicated the morphology of the Last Interglacial notch more efficiently

Abstract

Relic coastal landforms (fossil corals, cemented intertidal deposits, or erosive features carved onto rock coasts) serve as sea-level index points (SLIPs) widely used to reconstruct past sea-level changes. Traditional SLIP-based sea-level reconstructions face challenges in capturing continuous sea-level variability and dating erosional outcrops, such as ubiquitous tidal notches, carved around tidal level on carbonate cliffs. We propose a novel approach to such challenges by using a numerical model of cliff erosion embedded within a Monte-Carlo simulation to investigate the most likely sea-level scenarios responsible for shaping one of the best-preserved tidal notches of the Last Interglacial age in Sardinia, Italy. Results align with Glacial Isostatic Adjustment model predictions, indicating that synchronized or out-of-sync ice-volume shifts in Antarctic and Greenland ice sheets can reproduce the notch morphology, with sea level confidently peaking at 6m. This new approach yields continuous sea-level insights, bridging gaps in traditional methods and illuminating past Interglacial sea-level dynamics.

Plain Language Summary

Scientists typically investigate the position of sea level in geological time using the elevation, age, and characteristics of fossil marine organisms living in shallow water (e.g., coral reefs), beach deposits, or erosional features that were formed near the sea level. However, these indicators offer only fragmented information in time and not a continuous sea-level record. To overcome this issue, we use a numerical model that reconstructs the shape of tidal notches (i.e., indentations created close to sea level in carbonate cliffs). We compare our model-generated notch shapes with the real shape of the tidal notch, and we produce a set of continuous sea-level histories that are more likely to have produced one of the best-preserved fossil tidal notches in the Orosei Gulf, Sardinia, Italy which has been carved during the Last Interglacial high stand, 125.000 years ago. Our findings suggest that whether the ice sheets in Antarctica and Greenland melted at the same time or separately, both scenarios could create the actual shape of the tidal notch we observe at present. It’s also very likely that the sea level may have reached up to 6 meters.

1 Introduction

Coastal features such as fossil corals (Thompson et al., 2011) or cemented intertidal beach deposits (Falkenroth et al., 2019) formed at or close to sea level during past Interglacials can be used as sea-level index points (SLIPs), providing essential insights on past sea-level histories and hence on the dynamics related to the waxing and waning of ice sheets during periods that serve as process analogs for the near future (Dutton et al., 2015). The conventional method of gathering paleo sea-level data from SLIPs involves determining their elevation and relationship with the former sea level (Shennan, 2015), dating them via radiometric methods (such as U series), and ultimately reconstructing a relative sea level (RSL) curve, detailing the local interplay by changing sea level and land motions of non-climatic origin (Kopp et al., 2009). Despite its widespread application across thousands of global sites (Rovere et al., 2023), this approach has two major drawbacks.

First, SLIPs at one location are hardly continuous through time, and are often remnants of the past high stand peaks, providing little insight into the variability of sea level throughout the Interglacial. Second, SLIPs such as shore platforms (Trenhaile, 2001) or tidal notches (Antonioli et al., 2018) are ubiquitous but erosional in nature, hence they can be dated only indirectly, through stratigraphic correlation with deposits of known age. In this study, we suggest a novel solution that may help overcome the limitations of the traditional paleo sea-level analysis by reversing the conventional approach.

We begin by surveying with high-precision methods the morphology of a very well-preserved, laterally continuous tidal notch that formed during the warmest peak of Marine Isotope Stage 5 (MIS5e), the Last Interglacial (LIG - 125 ka BP) in the Orosei Gulf (Sardinia, Italy, NW Mediterranean) (Georgiou et al., 2020). A tidal notch is an indentation carved on steep carbonate cliffs and is typically situated near the mean sea level. In regions with micro- and meso-tidal ranges, like the Mediterranean Sea, tidal notches exhibit their greatest concavity proximal to the intertidal zone (Antonioli et al., 2018). Their genesis is attributed to a combination of active processes such as bioerosion, wetting and drying cycles, mechanical wave erosion, and hyperkarst (Trenhaile, 2015), which determine the rate of erosion. The width of the tidal notches, defined as the distance between their floor and roof, is predominantly controlled by the magnitude of the tidal range (Pirazzoli et al., 1991). Meanwhile, sea level stabilization or slowdown time, and whether the site is exposed or not (Vacchi et al. 2022) determines the incision depth and the width of the tidal notches, shaping the overall notch morphology (Trenhaile, 2016). Hence, fossil notches are frequently employed as SLIPs (Antonioli et al., 2015; Pirazzoli, 1986, 2005).

By incorporating a numerical model of cliff erosion (modified after Schneiderwind et al., 2017) with sea level as a fluctuating parameter, we use a Monte-Carlo approach (Eckhardt, 1987) to fit the model results with the measured notch geometry while accounting for the active processes involved in notch formation (Georgiou et al., 2020). We show that our best-fitting results closely align with the relative sea level predicted by Glacial Isostatic Adjustment (GIA) models at this locality (Stocchi et al., 2018). By imposing higher-than-present cliff erosion rates, we can force the model to reproduce two or three separate sea level peaks, which can be attributed to ice-volume change asynchrony between the Antarctic and Greenland ice sheets (Dumitru et al., 2023; Rohling et al., 2008, 2019). We provide a novel perspective into the interpretation of erosional sea-level indicators morphology, subsequently offering an insight into the intra-high stand sea-level variability and the notch formation mechanisms.

2 Methodological Approach

2.1 Photogrammetric Data Collection & Evaluation

The tidal notch of Orosei was surveyed during the summer of 2019. The survey was conducted using a boat navigating parallel to the cliff on a day with a calm sea and at low tide. Sequential photos of the cliff were acquired using a CANON D300 Reflex camera and were analyzed with Structure from Motion and Multi-View Stereo techniques (SfM-MVS) implemented into Agisoft Metashape (www.agisoft.com, see Supporting Information Text S1 for details, Carrivick et al., 2016; Casella et al., 2016; Ullman, 1979). The model was scaled using metric scale bars located on the cliff and was reduced to mean sea level using as a reference the inner part of the modern notch.

The 3D model was then imported into ArcGIS 10.1 where the geometry of the notch was extracted as a series of cross-profiles (Fig. 1a, Fig. 3). We highlight that the morphology of the notch is not uniform along its lateral extent since local factors are altering its depth, initial cliff plane, and notch floor extension. Through the geomorphometric analysis of the cliff's Digital Elevation Model (DEM), it was possible to discriminate the notch segments that were not well-preserved due to the presence of flowstone-like calcite formations or calcite accretion, differential erosion, and cliff collapse associated with rockfalls. This was achieved by using geomorphometric analysis including terrain attributes such as slope, aspect (Florinsky, 2017; Horn, 1981; Olaya, 2009), surface roughness (Sappington et al., 2007) as well as the cliff's color distribution (see Supporting Information-Figure S1, Text S2). Vertical profiles, called hereafter 'Measured Notch Profiles' were derived from the 3D model by averaging the point cloud at 1m intervals along the y-axis in the remaining areas.

2.2 Notch Reconstruction Model

Few static models have attempted to simulate the formation of a notch (Evelpidou et al., 2011, 2012; Larson et al., 2010; Pirazzoli, 1986; Trenhaile, 2014, 2015, 2016). To reconstruct the geometry of the measured notch at Orosei we modified the model of Schneiderwind et al., 2017 who coded a numerical model that integrates variables such as sea level change, erosion rate, tidal range, tectonics, and initial cliff inclination. This model employs a quadric polynomial equation (Equation 1) which simulates the development of a tidal notch through a parabola whose shape is determined by the variables shown in Figure 1a - (i) Erosion Rate (ER), (ii) Tidal Range (TR), (ii) Sea Level Curves (SLC), (iv) Initial Cliff Inclination (ICI), (v) Measured Notch Profiles (MNP).

$$f = \frac{ER*dt}{SLC-TR} * (notch\ height - SLC)^2 + ER * dt + ICI \text{ (Equation 1)}$$

The depth of the parabola defined by the equation, which is considered representative of the depth of the notch, is controlled by the erosion rate (ER) (Fig. 1a-i) after 1 year at mean sea level, while the width (defined as the distance between the notch floor and roof) is regulated by the tidal range (TR) (Fig. 1a-ii) and the fluctuation of the sea level curve (SLC) (Fig. 1a-iii). The inclination of the initial cliff, where the parabola begins to form, ranges from vertical to inclined (Fig. 1a-iv) depending on which notch profile from the measured ones on the field (MNP) (Fig. 1a-v) was selected to compare our modeled results. We inserted this equation in a Monte Carlo loop (Fig. 1c) which generates one million random combinations of the variables described (example shown in Fig. 1d) and by feeding them into Equation 1, it produces one million random notch simulations. The modeled notches that better fitted (≥80%) the measured notches were saved through each code iteration (Fig. 1e). More specifically the selected range of each parameter's values was constrained as follows:

i. Erosion Rate (ER): In our simulation, the depth of the tidal notch is determined by the erosion rate, which is the cumulative effect of all the active erosional processes taking place within the bounds of the tidal cycle. A range of 0.1 and 2mm/a of erosion was considered based on micro-erosion measurements and the carving depth of currently forming tidal notches across limestone cliffs in the Mediterranean Sea (Antonioli et al., 2015; Boulton & Stewart, 2015; Evelpidou & Pirazzoli, 2016; Furlani et al., 2014; Furlani & Cucchi, 2013; Pirazzoli & Evelpidou, 2013). ER used in the simulation was selected randomly for each iteration between the following values 0.25, 0.5, 0.75, 1, and 2, and is expressed as the parabolic erosion in millimeters per annum (mm/a).

ii. Tidal Range (TR): The notch's width for each annual tidal cycle was determined by the TR which was constant and analogous to the present TR (0.5m), based on the closest local tide gauge in Cagliari (www.mareografico.it, ISPRA). We retained the current TR for our analysis, based on evidence suggesting that tidal range variations are more pronounced with regions characterized by shallow shelves (Lorscheid et al., 2017), while deeper continental shelves demonstrate reduced susceptibility to tidal range changes under higher MIS 5e sea level conditions.

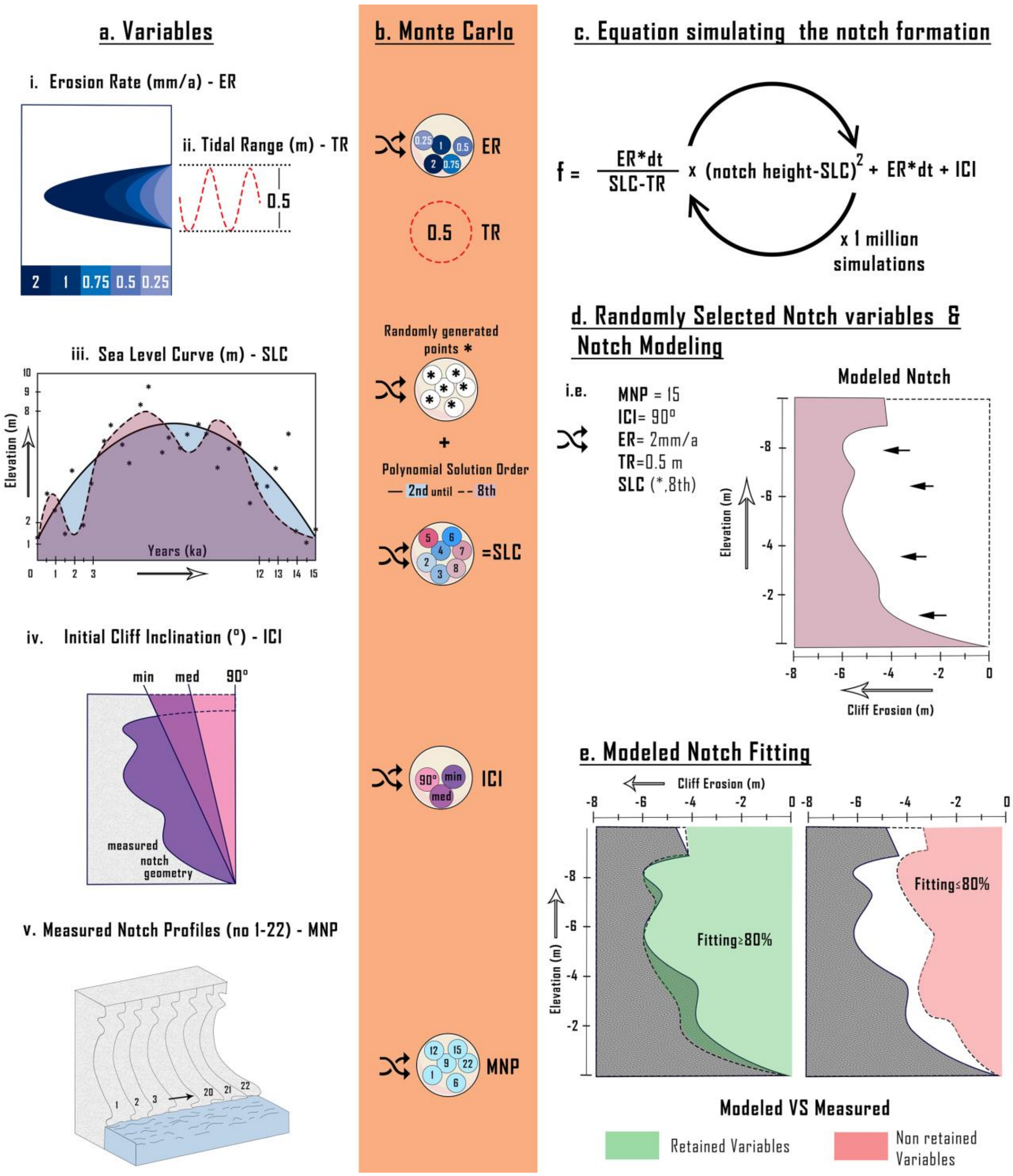

Figure 1. Model Workflow: a. Variables used in the equation: i. Erosion Rate range in mm/a, ii. Tidal Range: 0.5m (constant), iii. Sea Level Curve produced through random points interpolation using 2nd to 8th polynomial solution order, iv. Initial Cliff Inclination where the notch started to form, v. Measured Notch Profiles (MNPs) measured through SfM-MVS, b. Randomly Selected Variables through Monte Carlo simulation, c. Equation used for the notch modeling looped 1 million times, d. Example of the modeled notch simulated from their random combination, e. The variables producing a notch fitting higher or equal to 80% to the MNPs were retained (Software available in Georgiou N. (2023a), https://doi.org/10.5281/zenodo.8407427).

iii. Sea Level Curves (SLC): The shape of the notch was modeled using randomly generated SLCs of predetermined duration and height extent. To build each random SLC, random points were generated within a time window of 15 ka (to mimic the duration of MIS 5e, as per Polyak et al., 2018) at an equal interval of 500 years and an elevation range from 0-10m with a vertical interval precision of 10cm (Fig. 1a-iii). This sea-level range was selected to coincide with the maximum elevation of the Orosei notch above mean sea level (amsl), but also on the maximum reported sea level during the LIG (Dutton et al., 2015). For each simulation, the random points were interpolated into a curve using a randomly selected polynomial solution, ranging from the 2nd to the 8th order. In this way, sea level was allowed to fluctuate freely, giving rise to 1 million possible sea-level scenarios.

iv. Initial Cliff Inclination (ICI) & v. Measured Notch Profiles (MNP): The initial cliff plane used for the modeled notch to initiate its formation was derived from a randomly chosen notch profile chosen among 22 MNP (Fig. 1.a-v), acquired through SfM-MVS. Based on this random MNP, three inclinations were determined (Fig. 1.a-iv): minimum inclination (min) calculated using the hypotenuse between the seaward parts of the notch's roof and floor, straight vertical cliff (90°) starting at the most seaward part of the notch (floor or roof), and the median (med) inclination positioned between the minimum (min) and the vertical cliff (90°). The final inclination chosen for fitting was randomly picked from the min, med, or 90° options. The slope values derived from cliff mapping ranged between 60 to 90°.

2.3 Sea Level Curves Clustering

To assess the simulation outcomes and differentiate the modeled SLCs produced, we devised a clustering protocol that categorizes the most congruent SLCs according to their complexity. Since our model cannot yield results that define the timing of these events, it lacks the ability to discern between an early and a late sea-level rise, for each ER (0.25-2 mm/a) (Fig. 2a) we first used the Linear Regression statistical method to discriminate the SLCs based on their slope (positive (+) to negative (-), Fig. 2b). Subsequently, for every group identified, subgroups were formed based on the number of peaks present in each curve, categorizing the SLC types as single rise, 1 peak, 2 peaks, 3 peaks, or more than 3 peaks (Fig. 2c). While the sea level curve shapes for the scenarios involving one to three or more peaks are easily apprehensible, the single rise scenario which necessitates a consistent increase in sea level, requires that the sea level drop rate should always exceed the erosion rate to ensure the notch geometry remains unaltered. Finally, in each of these subgroups, the *K-means* unsupervised clustering algorithm (Lloyd, 1982) was employed (Fig. 2d). *K-means* clustering is an iterative algorithm that partitions a dataset into *k* distinct, non-overlapping clusters based on their similarities, aiming to minimize the variance within each cluster. The algorithm underwent multiple manual iterations, adjusting the number of clusters, to ascertain the optimal clustering outcome (best-fitting cluster). The best-fitting clusters as well as their scores are presented in Table S1 (Supporting Information).

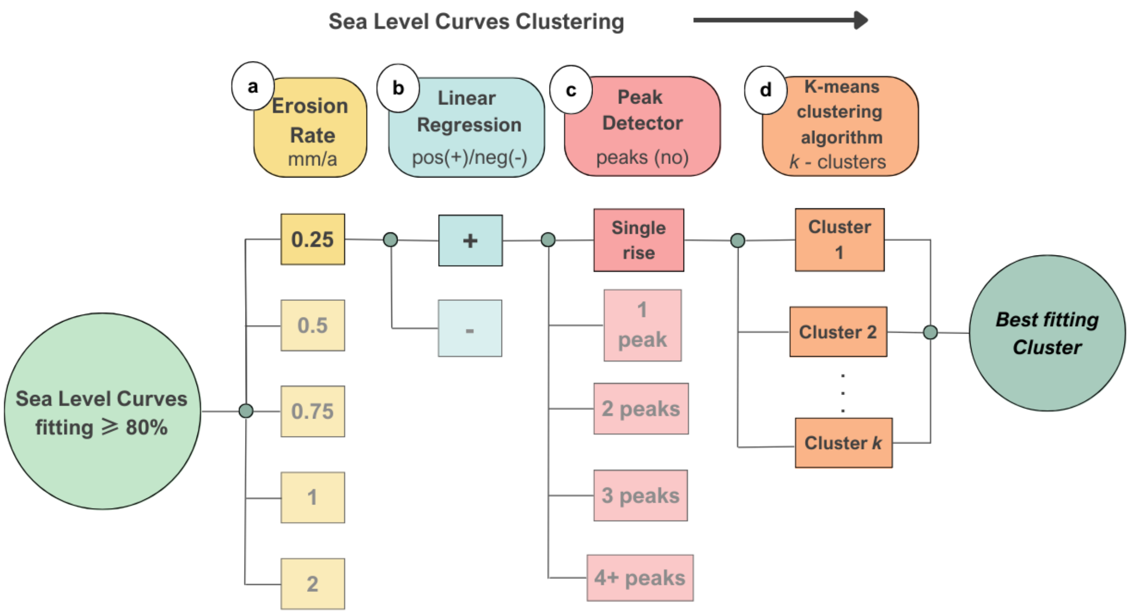

Figure 2. Sea Level Curves (SLCs) clustering workflow. SLCs generated from the numerical model (fitting ≥80%) were sub-grouped based on a. Erosion Rate (0.25-2 mm/a), b. Linear Regression (positive-negative direction), c. Number of Peaks (single rise, 1 to 4+peaks), d. K-means clustering (k-clusters), leads to the establishment of the best-fitting cluster for each subgroup.

3 Results

3.1 Tidal notch background and morphometry

The relic tidal notch carved on the cliffs of the Orosei Gulf stretches for about 70 km (Fig. 3a, b, d, e). The notch was carved by sea level during the LIG (Antonioli et al., 2006, 2018; Antonioli & Ferranti, 1992; Lambeck et al., 2004) on a Mesozoic carbonate cliff that stands at a height of up to 300m (D'Angeli et al., 2015). This is arguably one of the most well-preserved and laterally continuous tidal notches of this age on a global scale (Antonioli et al., 2006, 2018; Pirazzoli, 1986, 2005). Prior research attributes its exceptional preservation to burial by a continental talus, which prevented chemical dissolution and erosion after its formation (Antonioli & Ferranti, 1992). The mechanism behind the notch formation so far is believed to be the isostatic subsidence of the Western part of Sardinia during the LIG (Antonioli et al., 2006). Even though Sardinia is considered a tectonically stable site (Antonioli et al., 2015; Cerrone et al., 2021; Vacchi et al., 2018), MIS5e SLIPs detected in Orosei Gulf were recorded at a greater elevation compared to the rest of the island (+9.5m compared to +3.5-6m amsl, Fig. 3e). The lower elevations are detected at the SW and NW parts of Sardinia which were possibly affected by continental margin downthrow or fault-related subsidence. On the contrary, this height difference observed in Orosei Gulf is possibly linked to magmatic intrusion processes which uplifted our survey area about 2.4±0.2m (Mariani et al., 2009), presumably after the notch formation, since volcanic deposits younger than 125 ka BP were found filling MIS 5e lithophaga boreholes (Antonioli et al., 2006). Moreover, the uplifting factor further enhances the remarkable preservation observed in this case, since uplifted areas tend to preserve SLIPs in a better condition (Georgiou et al., 2022; Mattei et al., 2022; Pedoja et al., 2014). The Orosei notch geometry departs from the classic single parabolic indentation, displaying a ‘double notch’ morphology (Fig. 3c, d) as described by Antonioli et al. 2006.

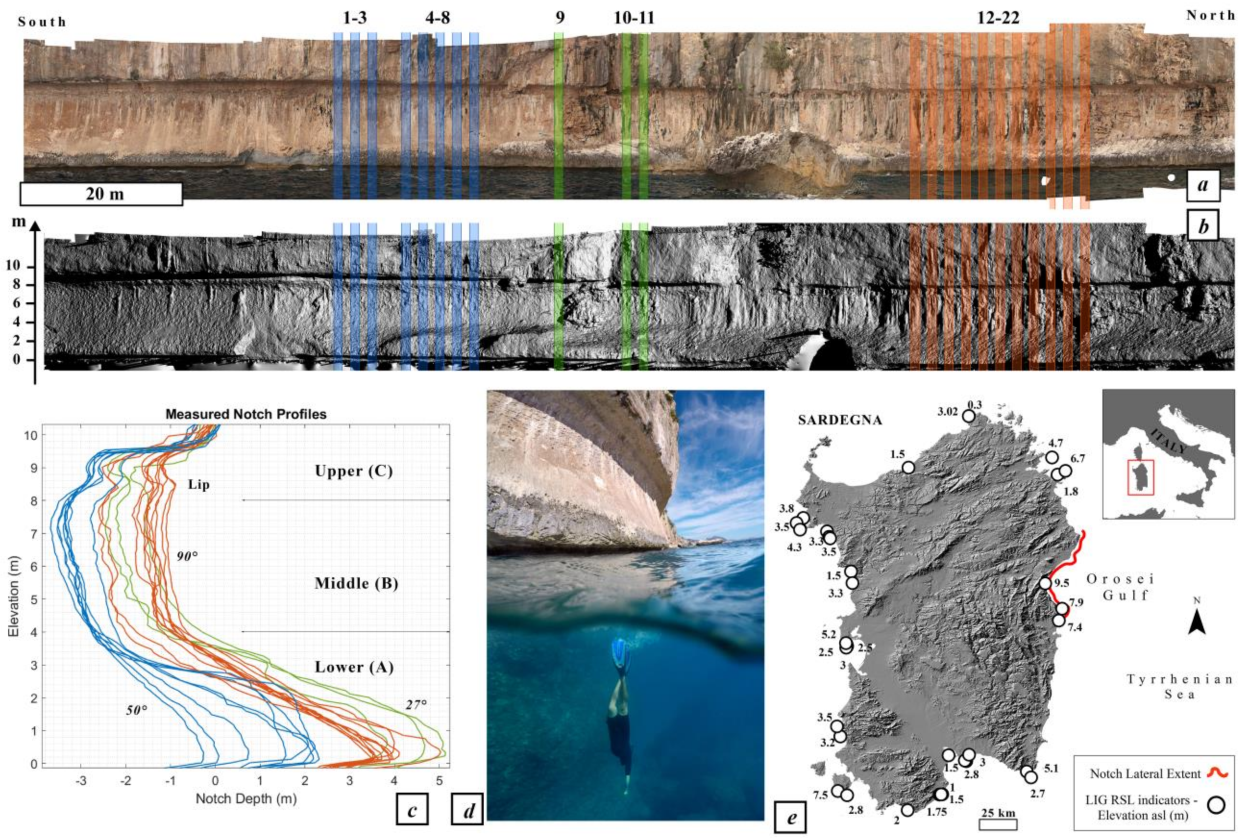

Figure 3. a. Notch orthomosaic carved on limestone cliff exposure of Orosei. Colored bands show the MNPs extracted for use in the numerical model. The colored bands represent MNPs with analogous characteristics (initial cliff inclination, notch floor seaward extension, notch depth), **b.** 3D hillshade model, **c.** MNPs used in the numerical model, **d.** ‘’over-under’’ photo showing the notch’s geometry, **e.** Hillshade elevation map of Sardinia, showing the notch lateral extension (red line) and the reported elevation amsl of MIS 5e RSL indicators (white dots) (Rovere et al., 2023).

3.2 Best-fitting Sea-level curves

We simulated the shaping of the Orosei notch by exploring 1 million combinations of the variables, as elaborated in the methodology (Fig. 1). Results with a high fit (≥80%) to the Measured Notch Profiles (MNPs) can be achieved by any scenario of initial cliff inclination. Instead, it was not possible to obtain high fit results using erosion rates (ER) akin to current ones (0.25 mm/a) (Table S1). To accurately represent the measured notch geometry, we had to impose a greater than modern ER (higher than 0.5 mm/a), which allowed obtaining a fit between modeled and measured notch profiles exceeding 80% (see Supporting Information for details, Table S1). In general, our results show that, as the complexity of SLCs increases, the fit of the modeled results with MNPs diminishes. The optimal average fit (83.8%) was obtained with an ER of 1 mm/a combined with the lowest SLC complexity (single rise). The same cluster yielded the overall best-fitting score of 91.6%. Notably, the second-best fit (90.1%) was produced when employing the 2mm/a ER scenario and under a 2-peak sea level scenario. However, the complexity of the SLC was irrelevant to the efficiency of the model under the highest ER scenario (2 mm/a) since both the lowest and highest complexity equally fitted the measured notch (83.3%).

Probability density plots of the sea level distribution (Fig. 4) were constructed for each cluster shown in Table S1 (Supporting Information). The distribution of the sea level (y-axis) is shown over a period of 15 ka (x-axis), providing an insight into the sea level variability during the LIG. The plots were weighted based on their fitting score, normalized from 0 to 1, and are described as low to high confidence distributions respectively.

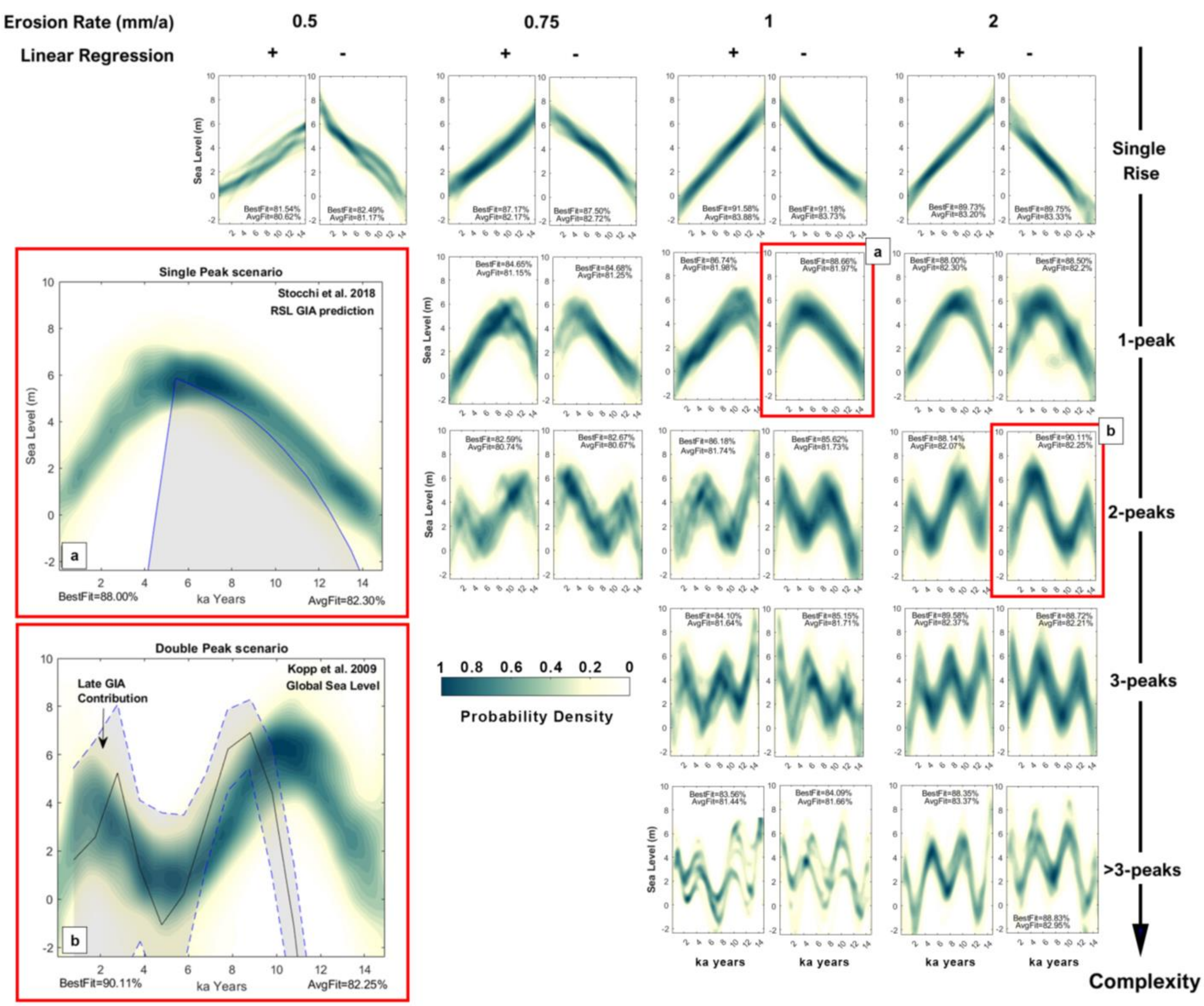

Figure 4. Probability density plots exhibiting the distribution of best-fitting sea level clusters (Table S1). Plots are grouped based on the Erosion Rate (0.5-2 mm/a) and the Linear Regression (positive-negative), while the SLCs complexity is increasing vertically (single rise, 1-peak,…, >3-peaks). Fig. 4. (a,b) Simulated sea-level probability

density plots in comparison to a. relative sea level (RSL) prediction based on GIA model from Stocchi et al. (2018), (concurrent melting of the Greenland Ice Sheet (GrIS) and Antarctic Ice Sheet (AIS)), b. probabilistic sea-level of Kopp et al. 2009, highlighting the asynchronous melting of the GrIS and AIS, coupled with the GIA subsidence during the later phase of the LIG (Data available in Georgiou N. (2023b), https://doi.org/10.5281/zenodo.8407819).

The findings indicate that an erosion rate (ER) of 0.5 mm/a, the closest to modern ERs, can effectively replicate the observed notch morphology (82.5%) only under the 'single rise' complexity scenario. In this scenario, the sea level rise rates vary between 0.3 to 0.8 mm/a, and the peak sea level is reached at 5.5 m. Fitting scores are significantly improving while increasing the ER (1 mm/a - 91.6% fitting) with sea level fluctuating more rapidly (0.5 to 1 mm/a).

The morphology of the Orosei notch could be replicated by the model also under a double-peak sea level scenario (maximum fitting of 90.1%), but only quadruplicating the ER (2 mm/a). In such cases, SLCs are characterized by a quick initial SLR rate (3.5-6 mm/a) followed by a short-lived sea level peak at 3.5-4 m. Shortly after, sea level drops to an elevation of 1m at a rate lower than 2 mm/a. Then, the sea level reaches a second peak through a relatively rapid sea level rise (1.5 mm/a), reaching a second peak at 6 m above modern sea level.

The same ER (2 mm/a) effectively replicated the measured notch morphology for increased complexity SLCs (3 peaks). These SLCs show three distinct peaks at heights of about 4, 5, and 6 m. Scenarios of even higher complexity, involving four peaks, diminish the efficacy of the simulations to a maximum of 88.8%, concurrently lowering the reliability of our sea level distributions.

4 Discussion

4.1 Simulated and predicted Sea-Level variability

The LIG vertical land movements in the Orosei Gulf were primarily modulated by the isostatic crustal response to surface loadings and secondarily by low-magnitude tectonic drivers that occurred after the development of the notch. According to GIA models, during the last phase of the LIG, the Central-Western part of the Mediterranean Sea and the Sardinian coasts were under the influence of isostatic subsidence (Antonioli et al., 2006; Lambeck et al., 2004; Stocchi et al., 2018), by virtue of water loading in the Tyrrhenian Sea. The prevailing belief is that this process was the principal mechanism behind the regional sea level rise during the formation of the notch, contributing to its enlarged geometry (Antonioli et al., 2006). By eliminating the post-uplifting factor (2.4m ±0.2, see Section 3.1), the sea level probability density distribution reveals that the combined contributions of eustatic and isostatic processes confidently yield a maximum paleo RSL value of 6 ± 0.2m (Fig. 4). This outcome remains consistent throughout all the model simulations irrespective of the variables utilized in constructing the SLCs. To add to this, this elevation aligns with the measured MIS5e RSL indicators surrounding the island of Sardinia (Fig. 3e).

Our best-fitting simulated SLCs were those exhibiting a single high stand peak scenario (complexity: single rise or 1 peak – ER: 1-2 mm/a), yet good-fitting results were obtained through the 0.5 mm/a ER scenario, which is more consistent with present-day ERs. These SLCs align closely with those predicted by the GIA models of Stocchi et al., 2018 for SE Sardinia, which model the simultaneous GrIS and AIS melting early in the interglacial (Fig. 4a). Our results are further reinforced by Antonioli et al., 2006 who surmised that the morphometry of the notch was merely attributed to late LIG isostatic subsidence, a process which is believed to have been reactivated during the MIS 1 (Vacchi et al., 2018). This result endorses the efficiency of our methodology for reconstructing the regional RSL based on the geometry of a tidal notch.

A double peak scenario showed exceptional fitting under an enhanced erosion rate scenario with two sea level peaks at 4 and 6m separated by a sea level drop close to 1m. The sea level distribution aligns closely with the global sea level range as predicted by Kopp et al. 2009. This would support the asynchronous ice sheet melting scenario with an early contribution of the AIS, followed by a low stand below modern sea level and a late simultaneous contribution of GrlS and AIS (Rohling et al., 2019, Dumitru et al., 2023). During the later phase of the LIG, glacial-isostatic subsidence of eastern Sardinia possibly co-contributed to the RSL rise (Fig. 4b). Relative SLIPs identified in the Western Mediterranean suggest that a double eustatic high stand scenario could bridge the differences between the predicted paleo RSL and observed superimposed fossil beach deposits (Hearty et al., 2007; Lorscheid et al., 2017). This is consistent with trends outlined in coral records(O'Leary et al., 2013; Thompson & Goldstein, 2005), corroborated by palaeoceanographic evidence (Grant et al., 2012; Rohling et al., 2019).

Finally, a rapidly fluctuating triple SL peak structure (Fig. 4) aligns closely with the probabilistic approach produced from the continuous indirect sea-level record of the KL11 and KL23 Red Sea sediment cores (Grant et al. 2012, Rohling et al., 2019). Although it is a plausible scenario, it remains to be supported through direct proxies since past abrupt sea level fluctuations may have left scarce direct traces, except for a triple reef structure in the Red Sea (Bruggemann et al., 2004).

4.2 Tidal notch formation mechanisms during the Last Interglacial (LIG)

Along the Mediterranean, limestone ERs have been reported to vary between 0.1 to 2 mm/a (Antonioli et al., 2015; Boulton & Stewart, 2015; Evelpidou & Pirazzoli, 2016; Furlani et al., 2014; Furlani & Cucchi, 2013; Karkani & Evelpidou, 2021; Pirazzoli & Evelpidou, 2013). Given the relative stability of the sea level in the last 3-4 ka, it's proposed that East Sardinia's limestones have an ER of 0.25-0.33 mm/a, as observed from modern tidal notch measurements (Antonioli et al., 2018; Vacchi et al., 2021). Our numerical model effectively replicated the observed notch using a minimum cumulative erosion rate (ER) of 0.5 mm/a., which is slightly higher than the modern one reported above.

Abrasion of the notch due to the presence of a sand beach was previously excluded (Antonioli et al., 2006), therefore one justification for the mismatch between the ER giving us the best results and measured ERs may reside in the fact that ERs could have been regionally increased, during the LIG, due to enhanced chemical dissolution from karst freshwater supply (Antonioli et al., 2006), greater bioerosion (Mottershead, 2013) or increased wave energy (Sunamura, 2019). Even if wave dynamics during the LIG period remain a complex subject of scientific inquiry, recent studies showed that warmer climate phases can affect both wave circulation patterns (Goodwin et al., 2023) and storm wave energy (Reguero et al., 2019; Wolf et al., 2020) thereby intensifying erosional processes and exerting significant mechanical force upon coastlines. Under these assumptions, our model results suggest that the tidal notch is indeed an MIS 5e relict (Antonioli et al., 2006) since it can be developed with a slightly higher ER compared to the present one (but included in the present ER range of 0.1-2 mm/a) and there is no need to invoke the effect of overprinting or reoccupation upon a previous sea-level high stand as detected in other study areas (Pastier et al., 2019; De Santis et al., 2023).

The initial cliff plane significantly influences notch geometry. Various initial cliff inclinations (60°-85° and 85°-90°) result in diverse notch shapes under uniform sea level changes. This confirms that notch asymmetries are linked to the initial cliff inclination (ICI) where the notch originated (Trenhaile, 2016), indicating that lower ICIs extend the notch floor.

5. Conclusions

In this study, we employed a simple numerical model to simulate the morphology of one of the best-preserved tidal notches dated to the LIG, in an attempt to reverse the classic workflow used to study past changes in sea level and derive, from a single sea-level indicator, a suitable set of sea level curves that can explain its morphology. While there are caveats to our modeling (discussed above), our results allow us to draw several conclusions.

1. Limestone erosion rates at our site might have been higher in the LIG. This follows from the fact that using modern erosion rates, our model has a low success rate in replicating the observed notch morphology under any combination of the other variables.

2. The highest fit between modeled and observed notch morphology is obtained with a LIG sea-level history characterized by a single sea-level peak. In this scenario, the sea-level history (in particular, the RSL rise rate) seems to coincide very well with RSL as reproduced by GIA models.

3. Using higher limestone erosion rates, our model can reproduce the notch profile under more complex LIG sea-level scenarios (2-peak, 3-peak), similar to those reported in the literature.

4. Under any model, we can reproduce the modern morphology of the notch by considering a slight post-tectonic uplift since the LIG. The peak sea level reached in any scenario is close to 6 m above present, which in our case would be the sum of eustatic (ice equivalent) sea level and post-depositional effects other than tectonics (i.e., GIA).

Acknowledgments

This work was co-funded by the European Research Council (ERC) under the European Union's Horizon 2020 research and innovation programme (Grant Agreement n. 802414-WARMCOASTS), the Erasmus+ Mobility Agreement and the PALSEA workgroup.

Open Research

The data are publicly available and archived in Zenodo: https://doi.org/10.5281/zenodo.8407819 licensed under Creative Commons Attribution 4.0 International . The scripts used for the numerical model and the figure production are made available in the open platform Github and archived in the Zenodo repository licensed under MIT License, https://doi.org/10.5281/zenodo.8407427 and can be cited as Georgiou N. (2023).

References

Antonioli, & Ferranti, L. (1992). Geomorfologia costiera e subacquea e considerazioni paleoclimatiche sul settore compreso tra S. Maria Navarrese e Punta Goloritzé (Golfo di Orosei, Sardegna). Giornale Di Geologia, 54(2), 66–89.

Antonioli, Ferranti, L., & Kershaw, S. (2006). A glacial isostatic adjustment origin for double MIS 5.5 and Holocene marine notches in the coastline of Italy. Quaternary International, 145–146, 19–29. https://doi.org/10.1016/j.quaint.2005.07.004

Antonioli, Lo Presti, V., Rovere, A., Ferranti, L., Anzidei, M., Furlani, S., et al. (2015). Tidal notches in Mediterranean Sea: a comprehensive analysis. Quaternary Science Reviews, 119, 66–84. https://doi.org/10.1016/J.QUASCIREV.2015.03.016

Antonioli, Ferranti, L., Stocchi, P., Deiana, G., Lo Presti, V., Furlani, S., et al. (2018, October 1). Morphometry and elevation of the last interglacial tidal notches in tectonically stable coasts of the Mediterranean Sea. Earth-Science Reviews. Elsevier B.V. https://doi.org/10.1016/j.earscirev.2018.06.017

Boulton, S. J., & Stewart, I. S. (2015). Holocene coastal notches in the Mediterranean region: Indicators of palaeoseismic clustering? Geomorphology, 237, 29–37. https://doi.org/10.1016/j.geomorph.2013.11.012

Bruggemann, J. H., Buffler, R. T., Guillaume, M. M. M., Walter, R. C., Von Cosel, R., Ghebretensae, B. N., & Bertie, S. M. (2004). Stratigraphy, palaeoenvironments and model for the deposition of the Abdur Reef Limestone: context for an important archaeological site from the last interglacial on the Red Sea coast of Eritrea. J.H. Bruggemann et al I Palaeogeography, Palaeoclimatology, Palaeoecology, 203, 179–206. https://doi.org/10.1016/S0031

Carrivick, M. W. Smith, & D. J. Quincey. (2016). Structure from motion in the GeoSciences. Retrieved from https://onlinelibrary.wiley.com/doi/

Casella, E., Rovere, A., Pedroncini, A., Stark, C. P., Casella, M., Ferrari, M., & Firpo, M. (2016). Drones as tools for monitoring beach topography changes in the Ligurian Sea (NW Mediterranean). Geo-Marine Letters, 36(2), 151–163. https://doi.org/10.1007/s00367-016-0435-9

Cerrone, C., Vacchi, M., Fontana, A., & Rovere, A. (2021). Last Interglacial sea-level proxies in the western Mediterranean. Earth System Science Data, 13(9), 4485–4527. https://doi.org/10.5194/essd-13-4485-2021

D'Angeli, I. M., Sanna, L., Calzoni, C., & De Waele, J. (2015). Uplifted flank margin caves in telogenetic limestones in the Gulf of Orosei (Central-East Sardinia-Italy) and their palaeogeographic significance. Geomorphology, 231, 202–211. https://doi.org/10.1016/j.geomorph.2014.12.008
Dumitru, O. A., Dyer, B., Austermann, J., Sandstrom, M. R., Goldstein, S. L., D'Andrea, W. J., et al. (2023). Last interglacial global mean sea level from high-precision U-series ages of Bahamian fossil coral reefs. Quaternary Science Reviews, 318, 108287. https://doi.org/https://doi.org/10.1016/j.quascirev.2023.108287
Dutton, A., Webster, J. M., Zwartz, D., Lambeck, K., & Wohlfarth, B. (2015). Tropical tales of polar ice: Evidence of Last Interglacial polar ice sheet retreat recorded by fossil reefs of the granitic Seychelles islands. Quaternary Science Reviews, 107, 182e196-196. https://doi.org/10.1016/j.quascirev.2014.10.025
Eckhardt, R. (1987). Stan Ulam, John von Neumann,and the Monte Carlo method. Los Alamos Sci.Spec. Issue, 15, 131–137.
Evelpidou, & Pirazzoli, P. A. (2016). Estimation of the intertidal bioerosion rate from a well-dated fossil tidal notch in Greece. Marine Geology, 380, 191–195. https://doi.org/10.1016/J.MARGEO.2016.04.017
Evelpidou, Pirazzoli, P. A., Saliège, J. F., & Vassilopoulos, A. (2011). Submerged notches and doline sediments as evidence for Holocene subsidence. Continental Shelf Research, 31(12), 1273–1281. https://doi.org/10.1016/j.csr.2011.05.002
Evelpidou, Vassilopoulos, A., & Pirazzoli, P. A. (2012). Submerged notches on the coast of Skyros Island (Greece) as evidence for Holocene subsidence. Geomorphology, 141–142, 81–87. https://doi.org/10.1016/j.geomorph.2011.12.025
Falkenroth, M., Schneider, B., & Hoffmann, G. (2019). Beachrock as sea-level indicator – A case study at the coastline of Oman (Indian Ocean). Quaternary Science Reviews, 206, 81–98. https://doi.org/10.1016/j.quascirev.2019.01.003
Florinsky, I. V. (2017). An illustrated introduction to general geomorphometry. Progress in Physical Geography: Earth and Environment, 41(6), 723–752. https://doi.org/10.1177/0309133317733667
Furlani, S., & Cucchi, F. (2013). Downwearing rates of vertical limestone surfaces in the intertidal zone (Gulf of Trieste, Italy). Marine Geology, 343, 92–98. https://doi.org/10.1016/J.MARGEO.2013.06.005
Furlani, S., Ninfo, A., Zavagno, E., Paganini, P., Zini, L., Biolchi, S., et al. (2014). Submerged notches in Istria and the Gulf of Trieste: Results from the Geoswim project. Quaternary International, 332, 37–47. https://doi.org/10.1016/j.quaint.2014.01.018
Georgiou, N., Rovere, A., Stocchi, P., & Casella, E. (2020). Reconstructing past sea level through notches: Orosei Gulf. In IMEKO TC-19 International Workshop on Metrology for the Sea. Retrieved from https://www.imeko.org/publications/tc19-Metrosea-2020/IMEKO-TC19-MetroSea-2020-35.pdf
Georgiou, N., Geraga, M., Francis-Allouche, M., Christodoulou, D., Stocchi, P., Fakiris, E., et al. (2022). Late Pleistocene submarine terraces in the Eastern Mediterranean, central Lebanon, Byblos: Revealing their formation time frame through modeling. Quaternary International, 638–639, 180–196. https://doi.org/https://doi.org/10.1016/j.quaint.2021.12.008
Georgiou N. (2023a). Nikos-Georgiou/TidalNotch_Generator_v1: TidalNotch Generator v1.0.0 (TidalNotchv1.0.0) [Software]. Zenodo. https://doi.org/10.5281/zenodo.8407427
Georgiou N. (2023b). Best-fitting Sea Level Curves generated from TidalNotch Generator model (v1.0.0) [Data set]. Zenodo. https://doi.org/10.5281/zenodo.8407819
Goodwin, I. D., Mortlock, T. R., Ribo, M., Mitrovica, J. X., O' Leary, M., & Williams, R. (2023). Robbins Island: The index site for regional Last Interglacial sea level, wave climate and the subtropical ridge around Bass Strait, Australia. Quaternary Science Reviews, 305. https://doi.org/10.1016/j.quascirev.2023.107996
Grant, K. M., Rohling, E. J., Bar-Matthews, M., Ayalon, A., Medina-Elizalde, M., Ramsey, C. B., et al. (2012). Rapid coupling between ice volume and polar temperature over the past 150,000 years. Nature, 491(7426), 744–747. https://doi.org/10.1038/nature11593
Hearty, P. J., Hollin, J. T., Neumann, A. C., O'Leary, M. J., & McCulloch, M. (2007). Global sea-level fluctuations during the Last Interglaciation (MIS 5e). Quaternary Science Reviews, 26(17–18), 2090–2112. https://doi.org/10.1016/j.quascirev.2007.06.019
Horn, B. K. P. (1981). Hill shading and the reflectance map. Proceedings of the IEEE, 69(1), 14–47. https://doi.org/10.1109/PROC.1981.11918
Kopp, R. E., Simons, F. J., Mitrovica, J. X., Maloof, A. C., & Oppenheimer, M. (2009). Probabilistic assessment of sea level during the last interglacial stage. Nature, 462(7275), 863–867. https://doi.org/10.1038/nature08686
Lambeck, K., Antonioli, F., Purcell, A., & Silenzi, S. (2004). Sea-level change along the Italian coast for the past 10,000 yr. Quaternary Science Reviews, 23(14–15), 1567–1598. https://doi.org/10.1016/j.quascirev.2004.02.009

Larson, M. P., Sunamura, T., Erikson, L., Bayram, A., & Hanson, H. (2011). An analytical model to predict dune and cliff notching due to wave impact. Coastal Engineering Proceedings, 1(32), sediment.35. https://doi.org/10.9753/icce.v32.sediment.35

Lloyd, S. (1982). Least squares quantization in PCM. IEEE Transactions on Information Theory, 28(2), 129–137. https://doi.org/10.1109/TIT.1982.1056489

Lorscheid, T., Stocchi, P., Casella, E., Gómez-Pujol, L., Vacchi, M., Mann, T., & Rovere, A. (2017). Paleo sea-level changes and relative sea-level indicators: Precise measurements, indicative meaning and glacial isostatic adjustment perspectives from Mallorca (Western Mediterranean). Palaeogeography, Palaeoclimatology, Palaeoecology, 473, 94–107. https://doi.org/10.1016/j.palaeo.2017.02.028

Lorscheid, T., Felis, T., Stocchi, P., Obert, J. C., Scholz, D., & Rovere, A. (2017). Tides in the Last Interglacial: Insights from notch geometry and palaeo tidal models in Bonaire, Netherland Antilles. Scientific Reports, 7(1). https://doi.org/10.1038/s41598-017-16285-6

Mariani, P., Braitenberg, C., & Antonioli, F. (2009). Sardinia coastal uplift and volcanism. Pure and Applied Geophysics. https://doi.org/10.1007/s00024-009-0504-3

Mattei, G., Caporizzo, C., Corrado, G., Vacchi, M., Stocchi, P., Pappone, G., et al. (2022). On the influence of vertical ground movements on Late-Quaternary sea-level records. A comprehensive assessment along the mid-Tyrrhenian coast of Italy (Mediterranean Sea). Quaternary Science Reviews, 279, 107384. https://doi.org/https://doi.org/10.1016/j.quascirev.2022.107384

Mottershead, D. (2013). 4.13 Coastal Weathering. Treatise on Geomorphology: Volume 1-14, 1–14, 228–244. https://doi.org/10.1016/B978-0-12-374739-6.00064-6

Olaya, V. (2009). Chapter 6 Basic Land-Surface Parameters. In T. Hengl & H. I. Reuter (Eds.), Developments in Soil Science (Vol. 33, pp. 141–169). Elsevier. https://doi.org/https://doi.org/10.1016/S0166-2481(08)00006-8

O'Leary, M. J., Hearty, P. J., Thompson, W. G., Raymo, M. E., Mitrovica, J. X., & Webster, J. M. (2013). Ice sheet collapse following a prolonged period of stable sea level during the last interglacial. Nature Geoscience, 6(9), 796–800. https://doi.org/10.1038/ngeo1890

Pastier, A.-M., Husson, L., Pedoja, K., Bézos, A., Authemayou, C., Arias-Ruiz, C., & Cahyarini, S. Y. (2019). Genesis and Architecture of Sequences of Quaternary Coral Reef Terraces: Insights From Numerical Models. Geochemistry, Geophysics, Geosystems, 20(8), 4248–4272. https://doi.org/https://doi.org/10.1029/2019GC008239

Pedoja, K., Husson, L., Johnson, M. E., Melnick, D., Witt, C., Pochat, S., et al. (2014). Coastal staircase sequences reflecting sea-level oscillations and tectonic uplift during the Quaternary and Neogene. Earth-Science Reviews, 132, 13–38. https://doi.org/https://doi.org/10.1016/j.earscirev.2014.01.007

Pirazzoli. (1986). Marine notches. Sea-Level Research: A Manual for the Collection and Evaluation of Data.

Pirazzoli. (2005). A review of possible eustatic, isostatic and tectonic contributions in eight late-Holocene relative sea-level histories from the Mediterranean area. Quaternary Science Reviews, 24(18–19), 1989–2001. https://doi.org/10.1016/J.QUASCIREV.2004.06.026

Pirazzoli, Laborel, J., Saliège, J. F., Erol, O., Kayan, İ., & Person, A. (1991). Holocene raised shorelines on the Hatay coasts (Turkey): Palaeoecological and tectonic implications. Marine Geology, 96(3), 295–311. https://doi.org/https://doi.org/10.1016/0025-3227(91)90153-U

Pirazzoli, P. A., & Evelpidou, N. (2013). Tidal notches: A sea-level indicator of uncertain archival trustworthiness. Palaeogeography, Palaeoclimatology, Palaeoecology, 369, 377–384. https://doi.org/10.1016/j.palaeo.2012.11.004

Polyak, V. J., Onac, B. P., Fornós, J. J., Hay, C., Asmerom, Y., Dorale, J. A., et al. (2018). A highly resolved record of relative sea level in the western Mediterranean Sea during the last interglacial period. Nature Geoscience, 11(11), 860–864. https://doi.org/10.1038/s41561-018-0222-5

Reguero, B. G., Losada, I. J., & Méndez, F. J. (2019). A recent increase in global wave power as a consequence of oceanic warming. Nature Communications, 10(1), 205. https://doi.org/10.1038/s41467-018-08066-0

Rohling, Grant, K., Hemleben, C., Siddall, M., Hoogakker, B. A. A., Bolshaw, M., & Kucera, M. (2008). High rates of sea-level rise during the last interglacial period. Nature Geoscience, 1(1), 38–42. https://doi.org/10.1038/ngeo.2007.28

Rohling, Hibbert, F. D., Grant, K. M., Galaasen, E. V., Irvalı, N., Kleiven, H. F., et al. (2019). Asynchronous Antarctic and Greenland ice-volume contributions to the last interglacial sea-level highstand. Nature Communications, 10(1). https://doi.org/10.1038/s41467-019-12874-3

Rovere, A., Ryan, D. D., Vacchi, M., Dutton, A., Simms, A. R., & Murray-Wallace, C. V. (2023). The World Atlas of Last Interglacial Shorelines (version 1.0). Earth Syst. Sci. Data, 15(1), 1–23. https://doi.org/10.5194/essd-15-1-2023

De Santis, V., Scardino, G., Scicchitano, G., Meschis, M., Montagna, P., Pons-Branchu, E., et al. (2023). Middle-late Pleistocene chronology of palaeoshorelines and uplift history in the low-rising to stable Apulian foreland: Overprinting and reoccupation. Geomorphology, 421. https://doi.org/10.1016/j.geomorph.2022.108530

Sappington, J. M., Longshore, K. M., & Thompson, D. B. (2007). Quantifying Landscape Ruggedness for Animal Habitat Analysis: A Case Study Using Bighorn Sheep in the Mojave Desert. The Journal of Wildlife Management, 71(5), 1419–1426. Retrieved from http://www.jstor.org/stable/4496214

Schneiderwind, S., Boulton, S. J., Papanikolaou, I., Kázmér, M., & Reicherter, K. (2017). Numerical modeling of tidal notch sequences on rocky coasts of the Mediterranean Basin. Journal of Geophysical Research: Earth Surface, 122(5), 1154–1181. https://doi.org/10.1002/2016JF004132

Shennan, I. (2015). Handbook of sea-level research. In Handbook of Sea-Level Research (pp. 3–25). https://doi.org/https://doi.org/10.1002/9781118452547.ch2

Stocchi, P., Vacchi, M., Lorscheid, T., de Boer, B., Simms, A. R., van de Wal, R. S. W., et al. (2018). MIS 5e relative sea-level changes in the Mediterranean Sea: Contribution of isostatic disequilibrium. Quaternary Science Reviews, 185, 122–134. https://doi.org/10.1016/j.quascirev.2018.01.004

Sunamura, T. (2019). Cliffs, Erosion Rates. In C. W. Finkl & C. Makowski (Eds.), Encyclopedia of Coastal Science (pp. 398–403). Cham: Springer International Publishing. https://doi.org/10.1007/978-3-319-93806-6_71

Thompson, W. G., & Goldstein, S. L. (2005). Open-system coral ages reveal persistent suborbital sea-level cycles. Science, 308(5720), 401–404. https://doi.org/10.1126/science.1104035

Thompson, W. G., Allen Curran, H., Wilson, M. A., & White, B. (2011). Sea-level oscillations during the last interglacial highstand recorded by Bahamas corals. Nature Geoscience, 4(10), 684–687. https://doi.org/10.1038/ngeo1253

Trenhaile. (2014). Modelling tidal notch formation by wetting and drying and salt weathering. Geomorphology, 224, 139–151. https://doi.org/10.1016/j.geomorph.2014.07.014

Trenhaile. (2015, November 1). Coastal notches: Their morphology, formation, and function. Earth-Science Reviews. Elsevier B.V. https://doi.org/10.1016/j.earscirev.2015.08.003

Trenhaile. (2016). Modelling coastal notch morphology and developmental history in the Mediterranean. GeoResJ, 9–12, 77–90. https://doi.org/10.1016/j.grj.2016.09.003

Trenhaile, A. S. (2001). Modeling the effect of late Quaternary interglacial sea levels on wave-cut shore platforms. Marine Geology. Retrieved from www.elsevier.nl/locate/margeo

Ullman, S. (1979). The interpretation of structure from motion. Proceedings of the Royal Society of London. Series B, Containing Papers of a Biological Character. Royal Society (Great Britain), 203(1153), 405–426. https://doi.org/10.1098/rspb.1979.0006

Vacchi, M., Ghilardi, M., Melis, R. T., Spada, G., Giaime, M., Marriner, N., et al. (2018). New relative sea-level insights into the isostatic history of the Western Mediterranean. Quaternary Science Reviews, 201, 396–408. https://doi.org/10.1016/j.quascirev.2018.10.025

Vacchi, M., Joyse, K. M., Kopp, R. E., Marriner, N., Kaniewski, D., & Rovere, A. (2021). Climate pacing of millennial sea-level change variability in the central and western Mediterranean. Nature Communications, 12(1). https://doi.org/10.1038/s41467-021-24250-1

Wolf, J., Woolf, D., & Bricheno, L. (2020). Impacts of climate change on storms and waves relevant to the coastal and marine environment around the UK. MCCIP Science Review, 132–157. https://doi.org/10.14465/2020.arc07.saw